electronics

MDPI

Article

Regenerative Battery Charging Control Method for PMSM Drive without a DC/DC Converter

Sung-Tae Ko [1], Soon-Sun Park [2] and Jung-Hyo Lee [2,*]

[1] Kokam Co. Ltd., Suwon, Gyeonggi-do 15846, Korea; sungtaeko@kokam.com
[2] Department of Electrical Engineering, Kunsan National University, Gunsan, Jeollabuk-do 54150, Korea; budababy8@naver.com
* Correspondence: jhlee82@kunsan.ac.kr; Tel.: +82-63-469-4707

Received: 23 September 2019; Accepted: 4 October 2019; Published: 7 October 2019

Abstract: This paper illustrates regenerative battery charging control method of the permanent magnet synchronous motor (PMSM) drive without DC/DC converter. Conventional control methods for battery current and voltage control methods generally use a bidirectional DC/DC converter for regenerative control. The reason to use this DC/DC converter is the DC-Link current ripple of the inverter of is affected by switching of the inverter and the motor speed. This problem causes to use a low pass filter (LPF) for sensing the DC-link current, however, it occurs deteriorating the control performance. In this paper, battery current and voltage control methods using only the motor drive are illustrated. To control the DC-link current, power control is performed using the look-up table (LUT) data that are extracted from the experiment. In addition, an applicable method for the variable DC-link voltage of the proposed regenerative control method is illustrated.

Keywords: PMSM drive; regenerative control; battery charging control

1. Introduction

Electrical components in vehicles are continuously modified to suit specific needs and requirements, and enhance drive efficiency [1–3]. A variety of electrical systems are used in vehicles and operating motors to improve fuel efficiency and performance. However, this has led to a rise in electric power consumption, especially with the application of active steering, suspension systems, and braking devices; mechanical or hydraulic motors are being replaced by electric drive systems. A permanent magnet synchronous motor (PMSM) drive for integrated starter and generator (ISG), nevertheless, have certain advantages. It not only propels initial driving power, but also reduces fuel consumption with an idle stop and go function. An ISG implements regenerative braking, which improves fuel efficiency by recovering some of the energy lost during conventional braking [4–6].

The drive topology of a PMSM is shown in Figure 1a; however, for DC-link voltage stabilization or to charge the battery, a bidirectional DC-DC converter is placed between the battery and the motor drive [7]. The bidirectional DC-DC converter in Figure 1b controls power flow by using a battery management system (BMS) [8–16]. Therefore, the PMSM drive configuration in Figure 1b offers more battery stability and efficiency, as compared to the arrangement in Figure 1a.

As previously mentioned, the ISG drive provides the driving or braking force to the wheel, in an effort to increase efficiency of the traction drive. Regenerative control, which is an ISG application, generates a braking torque to provide a braking force and charge the battery [17]. This brake system has recently been improved upon to produce the hybrid brake, which combines mechanical and electrical braking features using an ISG to enhance the driving distance [17–22]. Figure 2 shows the control method of the hybrid brake: the main control unit (MCU) controls the brake torque (which is provided by the electrical and mechanical brakes), taking into consideration the battery's state of charge (SOC).

When the brake torque from the brake pedal is beyond the battery's capacity, MCU transfers the remaining brake torque to a mechanical brake controller. This hybrid system not only transfers brake energy back to the battery, but also enhances the mechanical brake's life by reducing abrasion.

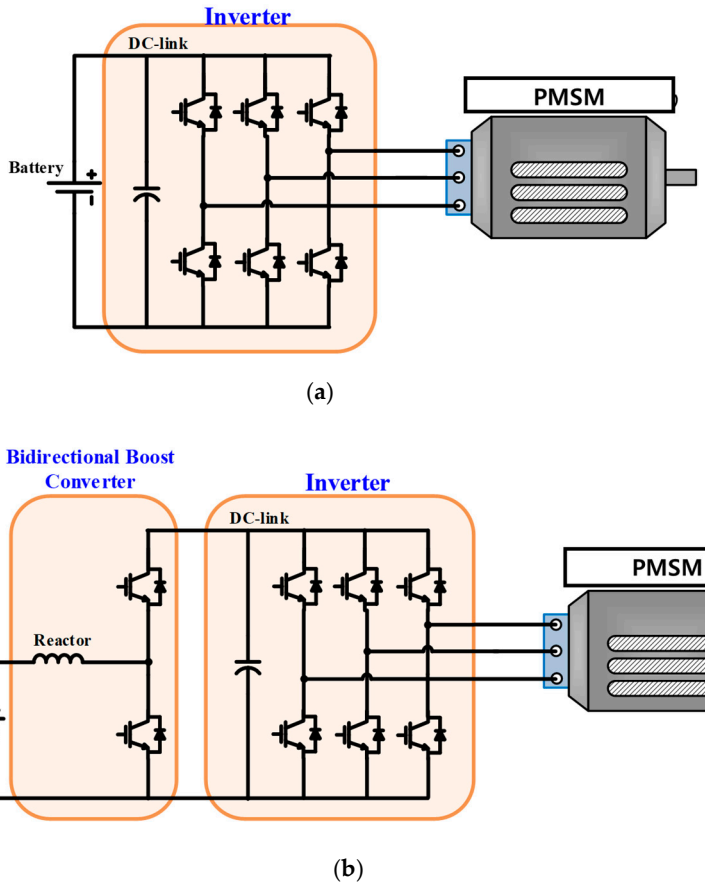

Figure 1. Power conversion unit of PMSM drive for regenerative control: (**a**) General topology of PMSM drive; (**b**) PMSM drive with DC-DC converter.

The hybrid brake is a fine technique; however, conventional research focuses only on increasing a vehicle's braking performance [18–22]—they use the topology shown in Figure 1a; the torque required to enhance braking performance is directly applied to PMSM drive, ignoring suitable battery charge that emanates from the BMS. Although braking performance is important, battery charge control is also vital, as it enhances battery life. Research on electric brake control using only motor drive is limited [23,24]; moreover, the studied control methods only consider battery voltage, not battery current.

Assuming that the MCU reflects battery SOC and current reference from the BMS, optimal charging current to the battery can be achieved by allocating a braking torque to the mechanical brake and ISG. Based on this concept, this paper proposes battery current and voltage control methods using PMSM drive. With the topology shown in Figure 1b, regenerative battery current and voltage control is easily achieved by using a DC/DC converter with the conventional battery charging control. However, as this topology needs additional switches and a reactor, the cost and size unavoidably increases. In contrast, the topology of Figure 1a struggles to control the charging current because the DC-link current of the inverter is degraded by switching and motor speed. A DC-link capacitor can mitigate this ripple; however, in cases of slow motor speed, this effect reduces. This paper first explains the PMSM torque control method using a look-up table (LUT) for current reference generation. It then elucidates the DC-link current sensing problem. In addition, the proposed regenerative control method for PMSM drive is illustrated. Finally, the proposed algorithm is verified by experimental results.

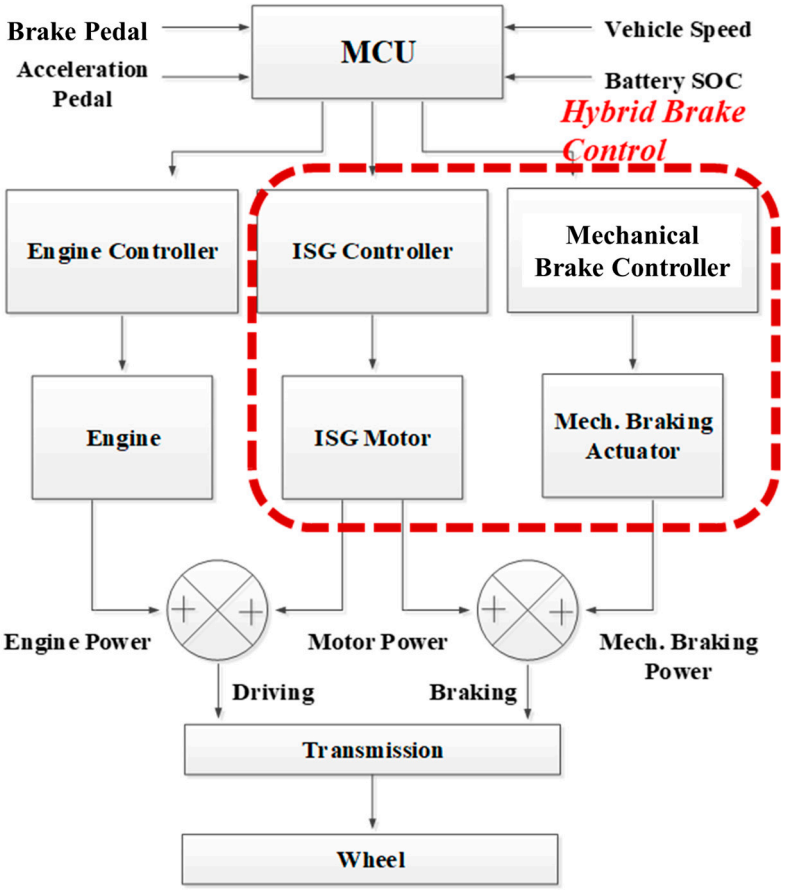

Figure 2. Hybrid brake control method for an ISG.

2. Regenerative Power of a PMSM

2.1. Torque Control of a PMSM

A three-phase PMSM is modelled by synchronous d-/q-axis transformation. The transformed electrical torque equation is expressed as:

$$T_e = \frac{3}{2}\frac{P}{2}\left(\phi_{pm} i^r_{qs} + (L_d - L_q) i^r_{ds} i^r_{qs}\right) \tag{1}$$

Electrical torque is the value that divides mechanical output by velocity. Therefore, power generated from the PMSM can be expressed as Equation (2), assuming that copper and iron loss can be negligible, caused by small fluctuations in the phase current ripple:

$$P_{out} = \frac{3P}{4}\omega_r\left(\phi_{pm} i^r_{qs} + (L_d - L_q) i^r_{ds} i^r_{qs}\right) \tag{2}$$

Based on the equation above, if the motor rotates in a forward direction at constant velocity and torque, the generated power is constant and has a positive value. Because inductance L_q is larger than L_d in an interior mounted PMSM (IPMSM), d-axis current should have a negative value in order to obtain a positive second term of Equation (2). On the other hand, power flow direction of the regenerative operation should be from the PMSM to the DC-link, and the q-axis current should be of a negative value to achieve the direction as described in Equation (2). The power from the PMSM to the DC-link can be expressed as follows:

$$P_{in} = V_{dc} I_{dc} \tag{3}$$

If the loss from inverter switching or friction of mechanical gear can be ignored, the power generated by the PMSM and the power transmitted to the DC-link will be the same. In this case, Equation (4) is deducted from Equations (2) and (3):

$$\begin{array}{c} P_{in} = P_{out} \\ V_{dc}I_{dc} = \frac{3P}{4}\omega_r\left\{\phi_{pm}i_{qs}^r + \left(L_d - L_q\right)i_{ds}^r i_{qs}^r\right\} \end{array} \quad (4)$$

As illustrated in Equation (4), regenerative power to the battery is controlled by PMSM current. Because DC-link voltage (V_{dc}) is always positive and motor speed of ISG (ω_r) is almost positive (except during reverse driving), the q-axis current and DC-link current generally are in the same direction. Therefore, a negative q-axis current can generate torque that is in the opposite direction of motor speed, and can generate regenerative power to the DC-link and the battery. Note that the negative DC-link current absorbs energy from the motor. Assuming that the capacitance of the battery is almost infinite, this absorbed energy is delivered to the battery through the DC-link due to the constant DC-link voltage. As a result, the negative DC-link current becomes the input current of the battery, thus charging it.

On the other hand, various d-/q-axis currents can generate specific torque and power, according to Equation (1). Specific torques identified according to Equation (1) can be expressed by various d-/q-axis current combinations, as shown in Figure 3. The most efficient current point is the maximum torque per ampere (MTPA) point, which points to the minimum current magnitude. As shown in the figure, generating and regenerating torques have a symmetrical relation to the q-axis. If the same amount of torque is generated or regenerated, the d-axis current for the MTPA point is the same and the q-axis current for the MTPA point only changes direction. Therefore, if the MTPA points of various motoring torques are identified, the MTPA points of regenerating torques are easily estimated.

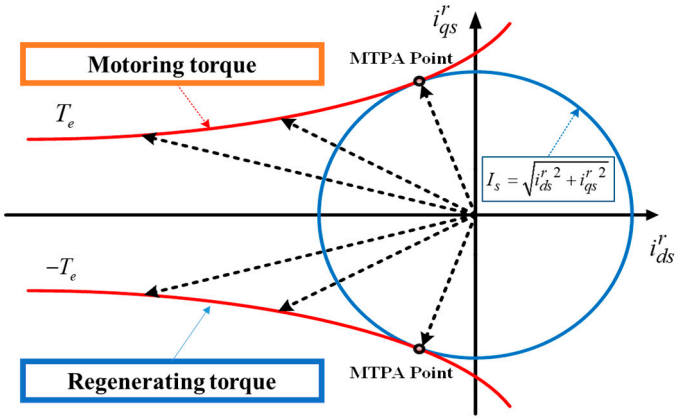

Figure 3. Combination of currents generated from the same torque.

Generally, these current points are stored in an LUT, wherein it responds to a specific torque command. However, if motor speed increases, these d-/q-axis current points should take into consideration MTPA points for torque generation and restriction of the back-EMF voltage. The back-EMF voltage amount can be calculated as below:

$$\begin{array}{l} E_{mag} = \sqrt{\left\{R_s i_{qs}^r + \omega_r(L_d i_{ds}^r + \phi_{pm})\right\}^2 + \left(R_s i_{ds}^r - \omega_r L_q i_{qs}^r\right)^2} \\ E_{mag} \le V_{\max}(V_{\max} = V_{dc}/\sqrt{3}) \end{array} \quad (5)$$

The ISG needs to satisfy a broad velocity region through a field weakening technique, which reduces the back-EMF voltage. However, the d-/q-axis current point for field weakening control is affected by PMSM parameters, as described in Equation (5), especially for resistor variation. Because the voltage drop caused by the resistor is easily changed by operating temperature or humidity, optimal

d-/q-axis currents for specific generating and regenerating torque in a field weakening region have large differences. Thus, current data in an LUT for a field weakening region is usually experimentally established. In addition, because the LUT has to reflect torque command as well as current speed for the field weakening operation, it needs to be two-dimensional (2D-LUT). Figure 4 shows the 2D-LUT of the ISG motor used in this paper.

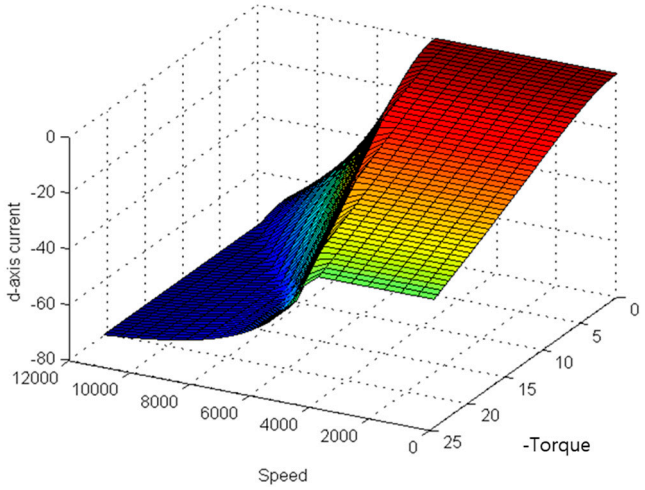

(**a**)

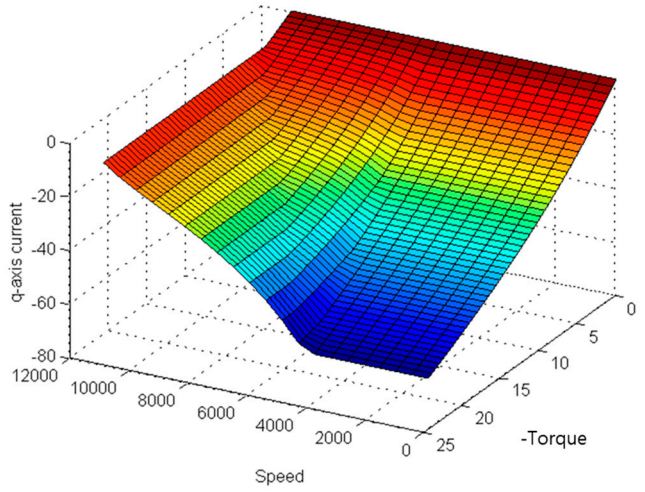

(**b**)

Figure 4. dq-axis current references for regenerative torque generation. (**a**) d-axis (**b**) q-axis

With these 2D-LUTs for the d-/q-axis current, instantaneous torque control can be achieved by using the vector control method—it is the most common control method for PMSM drive, generating torque by controlling the d-/q-axis current flowing through the stator phase current. In this case, d-axis is the position wherein magnetic flux is generated from the positive pole of the permanent magnet, and q-axis has a 90° phase difference from the magnetic flux of the rotor in space. Because the PMSM is a synchronous motor, the flux caused by the stator current has to be sync with motor speed. To achieve this, the stator current needs to be transformed by using the rotor reference frame, which rotates at the rotational velocity of the rotor. Position information of the rotor (θ_r) is required for synchronous frame transformation for vector control. In general, a position sensor is used to detect rotor position and the

obtained information transforms the three-phase currents to d-/q-axis currents, or d-/q-axis voltage references to three-phase voltage references.

Figure 5 shows a block diagram of the algorithm used for instantaneous torque control in a PMSM. As mentioned earlier, the current reference to generate specific torque for MTPA and field weakening operation is output using 2D-LUT. On using the identified torque, the battery can be charged through torque assist and regeneration of the ISG system. However, the conventional ISG system does not include a separate algorithm for effective charging of the battery [23,24]. It simply ensures voltage control—maintains nominal voltage—when there is an increase due to overcharging of the battery. However, such a control method is insufficient for efficient battery use, because it fails to have appropriate current control. In this case, the current sensor is simply used to detect the overcurrent flowing in the battery, instead of being used for current control.

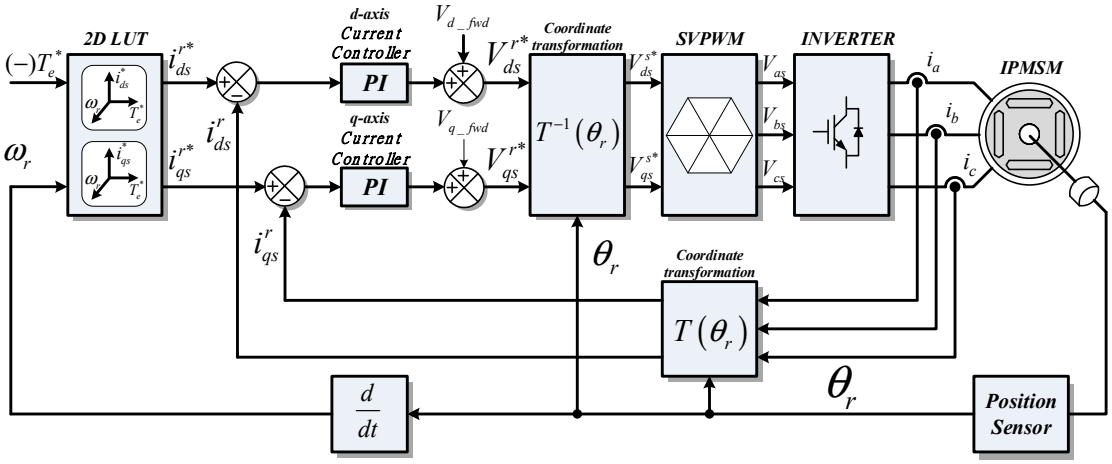

Figure 5. General regenerative torque control in a PMSM drive.

2.2. Problem of Sensing the DC-link Current

As aforementioned, the DC-link current in the three -phase inverter is affected by inverter switching and back-EMF voltage. One of the biggest problems with the conventional method is that the regenerative energy of the inverter cannot be estimated by DC-link current. As is widely known, the actual inverter DC-link current is corrupted by the switching of the inverter and the back-EMF voltage of the traction motor. A brief explanation of this current ripple is provided in this section.

To analyze this current ripple, a-phase output voltage of the inverter is modeled:

$$V_{an} = E_{an} + j\omega_r L_s i_a(t) \tag{6}$$

where, n is the PMSM neutral point, V_{an} is the a-phase inverter output voltage, E_{an} is the a-phase back-EMF voltage.

In the steady state, the fundamental component of the inverter output voltage is the same as that of the back-EMF voltage. The current ripple is calculated as:

$$i_{a\_ripple} = \frac{V_{an} - E_{an}}{j\omega_r L_s} \tag{7}$$

where, i_{a_ripple} is an a-phase current ripple.

Fundamentally, the inverter output voltage is not sinusoidal voltage, but rectangular pulse. Therefore, this voltage difference between the fundamental component and the real voltage creates the

current ripple. On the other hand, in an ideal condition, the input power of the DC-link would be the same as the output power.

$$V_{dc} i_{dc}(t) = v_{an}(t) i_a(t) + v_{bn}(t) i_b(t) + v_{cn}(t) i_c(t) \tag{8}$$

From Equation (7), instantaneous DC-link current can be obtained as:

$$\begin{aligned} i_{dc}(t) = \tfrac{E_{mag} I_a}{V_{dc}} [&\cos(\omega_r t)\cos(\omega_r t - \phi) \\ &+ \cos(\omega_r t - 120°)\cos(\omega_r t - \phi - 120°) \\ &+ \cos(\omega_r t + 120°)\cos(\omega_r t - \phi + 120°)] \end{aligned} \tag{9}$$

where, E_{mag} and I_a are the amplitudes of the phase voltages and the currents, respectively, and ϕ is the phase difference between the phase voltage and the current.

From this equation, it can be seen that instantaneous DC-link current is affected by motor back-EMF; the DC-link current has the 6th harmonic component. Therefore, Equation (9) can be approximately transformed to the following equation:

$$\begin{aligned} i_{dc}(t) &= \tfrac{3E_{mag} I_a}{V_{dc}} \cos\phi + k_1 \tfrac{3E_{mag} I_a}{V_{dc}} \cos(6\omega_r t - \phi) + k_2 i_{SW}(t) \\ &= I_{dc} + \widetilde{i}_{DC1}(t) + \widetilde{i}_{DC2}(t) \end{aligned} \tag{10}$$

where, k_1, k_2 are the magnitude gains of the DC-link current ripples.

In Equation (10), the first component I_{dc} is the DC component, which relates to regenerative energy. The second component $\widetilde{i}_{DC1}(t)$ is the 6th harmonics component, which is a result of the back-EMF and DC-link voltage. The third component $\widetilde{i}_{DC2}(t)$ is the switching current ripple. On observing the DC-link current, it can be seen that the switching current ripple $\widetilde{i}_{DC2}(t)$ can be removed by LPF. However, the harmonic component $\widetilde{i}_{DC1}(t)$ cannot be easily disconnected because harmonic frequency varies according to the DC-link capacitor, and swelling of the current remains at low speed. Besides, this capacitor is only operated as an LPF, which has a specific low value cut-off frequency. Therefore, control dynamics are restricted when the DC-link current is controlled by a sensing current. Figure 6 illustrates Equation (10): the period of $\widetilde{i}_{DC1}(t)$ and $\widetilde{i}_{DC2}(t)$ are well described, highlighting that $\widetilde{i}_{DC1}(t)$ is six times that of the phase current period and $\widetilde{i}_{DC2}(t)$ is the switching period.

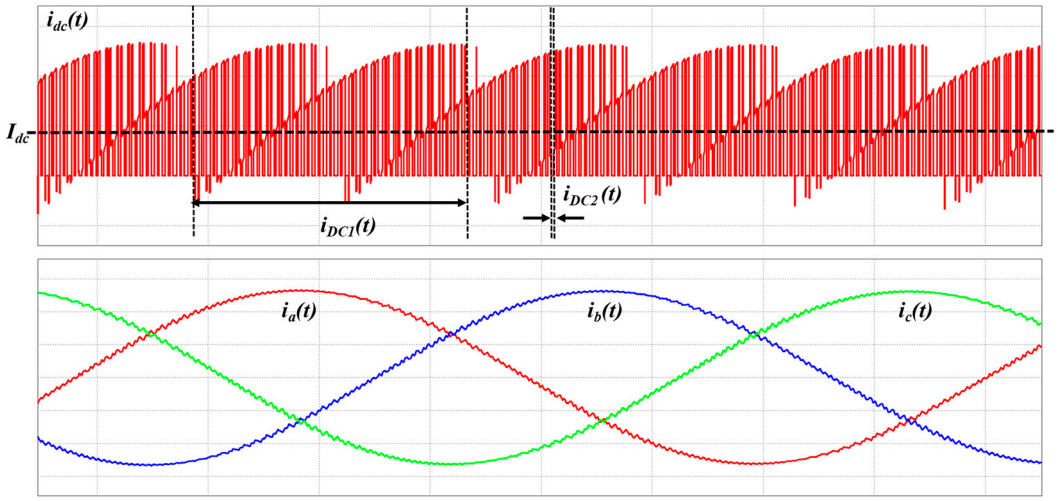

Figure 6. Analysis of the DC-link current ripple.

Fortunately, DC-link current's ripples decrease in relation to the value of DC-link capacitance. In the manufacturing of traction drives, capacitance value is set at more than 10 times the designated value, because reduction in a battery charging current's ripples enhances the life of a PMSM drive

system. However, an ISG drive does not allow such a size or cost. In order to meet these restrictions, a designated capacitance has to be applied to PMSM drive, without any margins. This does not allow the charging current's sensor to use low pass filter (LPF) that has low cut-off frequency. This affects control performance owing to slow sensing data acquisition, thus degrading the battery's constant current (CC) control performance. Moreover, as previously mentioned, the frequency of the ripples vary with motor speed, and controller gain setup for stable operation is performed under adverse conditions.

3. Proposed Regenerative Control Method for Battery Charge

We will first explain the constant current and voltage control method for battery charge using a general DC-DC converter. Using the configuration shown in Figure 1a, battery current and voltage can be substituted by DC-link current and voltage. Figure 7a shows the general constant voltage (CV) and a constant current control block; operation of this block is shown in Figure 7b. In Figure 7, the DC-link voltage is controlled by a PI controller. The output of the voltage controller is limited by the desired current reference for CC control operation. During the CC control operation, because the target voltage does not reach the reference, the voltage controller output is saturated by the PI controller. The desired current reference for the CC operation is then inserted into the limiter to adjust the saturated voltage controller output. This saturated current reference is input into the current controller to control the battery current. If the battery voltage reaches the reference value, the saturated voltage controller is released, and CV control is initiated. CV operation reduces the battery current, and subsequently the voltage drop by battery impedance is also decreased. Consequently, the open terminal voltage of the battery is set as the voltage reference. Figure 7b shows the CC-CV control result.

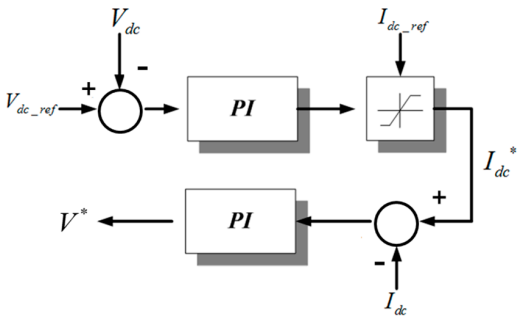

(**a**)

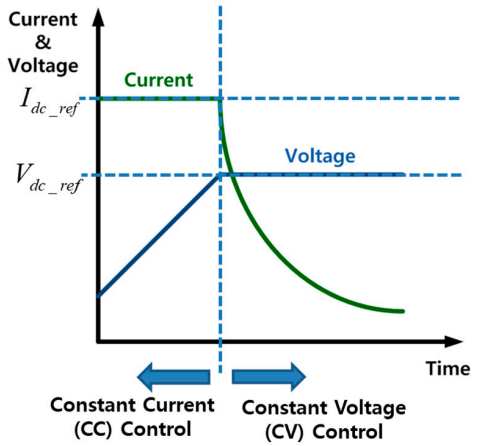

(**b**)

Figure 7. Constant current (CC) and constant voltage (CV) controls: (**a**) General CC-CV controller block diagram; (**b**) CC-CV control operation.

As previously mentioned, DC-link current has lots of ripples, created by the switching power converter and voltage of back-EMF. Therefore, if this general CC-CV controller is adopted in a PMSM drive system, the problem of DC-link current sensing arises. To solve this problem, this paper proposes an indirect DC-link current control by means of a power controller. Figure 8 shows the proposed control method.

As a conventional current and voltage controller, the voltage controller generates the current reference. However, the DC-link current reference is multiplied by the current DC-link voltage to deduct the power reference. The generated power reference is compared with the PMSM regeneration power based on a simple equation:

$$V_{dc}I_{dc} = K(T_e, \omega_r) \times T_e\omega_r \tag{11}$$

where, $K(T_e,\omega_r)$ is the efficiency of the energy transformation from mechanical energy to electrical energy.

As is widely known, the efficiency of a PMSM operation varies with generation torque and motor speed. Therefore, the proposed control method needs two LUT data: the first is the generated torque, and the second is efficiency. Generated torque can be estimated by dq-axis current, based on Equation (1). Note that the generated torque is only affected by current, not motor speed. Figure 9 shows the estimated torque with dq-axis currents.

On the other hand, the efficiency of PMSM drive is affected by copper and iron losses. Copper loss is the dissipation of energy caused by nonlinearity between the current and flux—hysteresis and eddy current losses. Therefore, this loss is proportional to motor speed. Iron loss is the loss caused by resistance of the windings. Therefore, this loss is proportional to motor current. As a result, to achieve correct power control, parameter K has to consider motor speed and torque. Figure 10 shows the estimated efficiency of the target motor drive, according to motor speed and torque.

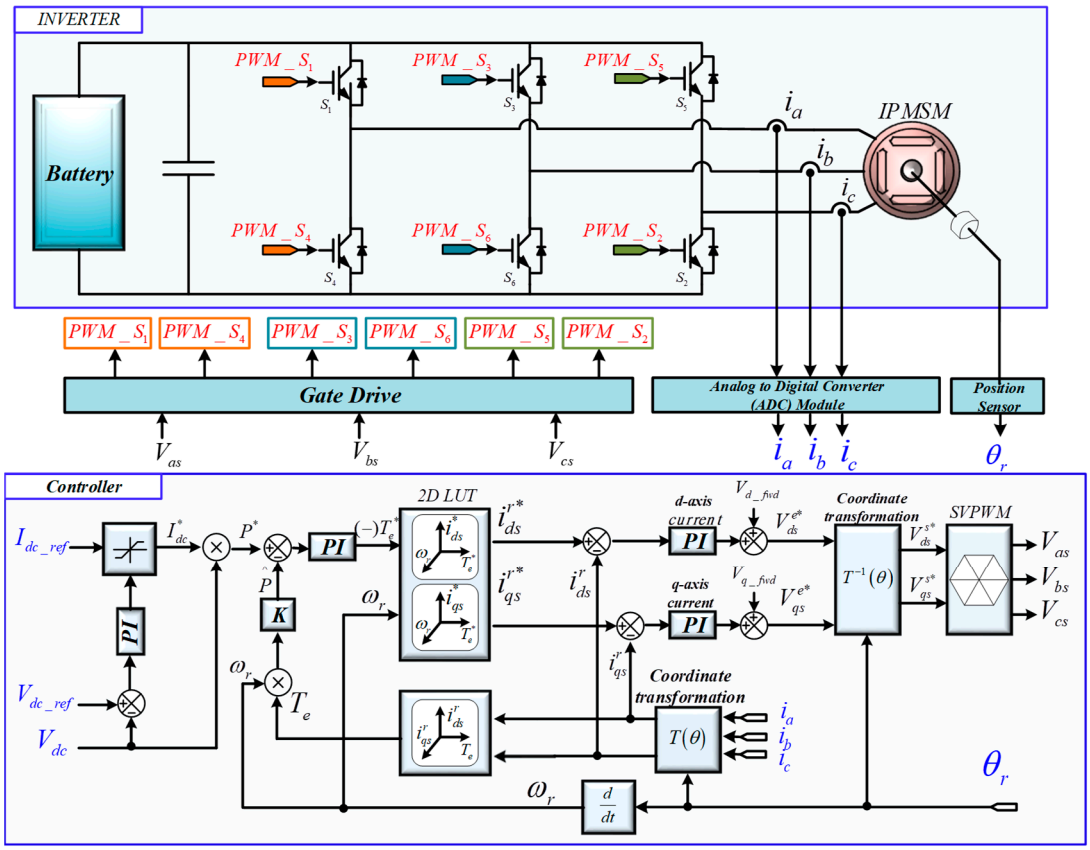

Figure 8. The proposed regenerative battery charging control method without a DC/DC converter.

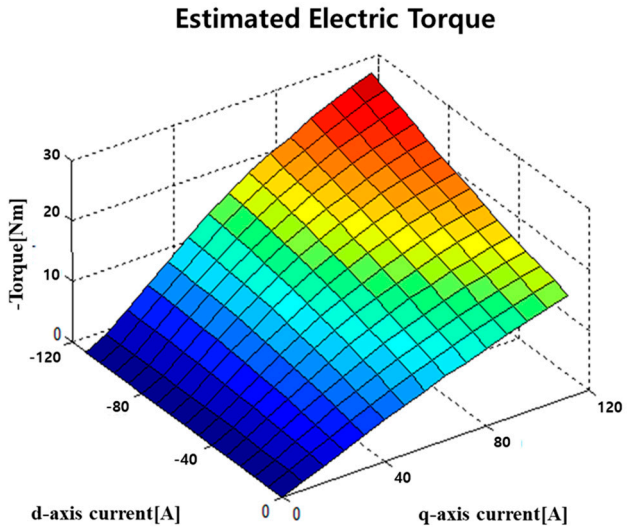

Figure 9. Estimated electric torque according to d-/q-axis currents.

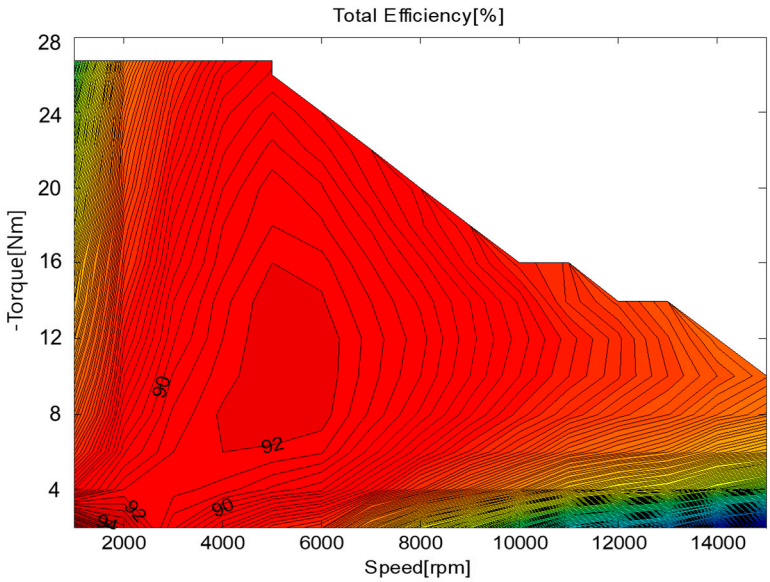

Figure 10. Efficiency of the target motor drive.

4. Experimental Results

In order to verify the validity of the CC-CV regenerative control in an ISG system, we created an experimental setup (Figure 11). The target PMSM drive parameters are provided in Table 1 and battery parameters in Table 2.

Table 1. PMSM drive parameters.

Parameter	Value
Pole	8
Permanent magnet flux	0.0045 (Wb)
d-axis inductance	0.000303 (H)
q-axis inductance	0.000907 (H)
Resistance	0.0003 (Ω)
DC-link capacitance	670 (μF)
Rated phase current	110 (A)
Rated Speed	4800 (rpm)
Rated Torque	32 (Nm)

Table 2. Battery parameters.

Parameter	Value
Battery type	LiB
Rated voltage	250 (V)
Rated current	18 (Ah)
Maximum charging current	28 (A)

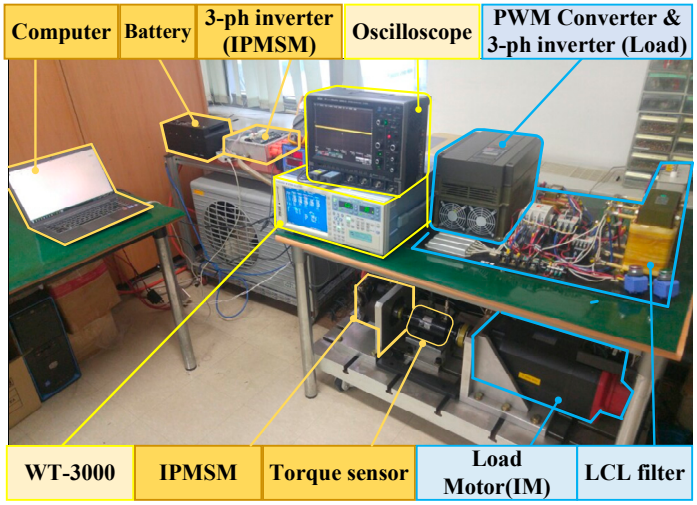

Figure 11. Experimental setup.

Figure 12 provides the results of the CC-CV control; Figure 12a shows the battery current and voltage, Figure 12b shows the three-phase currents during the CC-CV operation. Load motor is coupled with a target PMSM to ensure that motor speed is the rated 4800 rpm, and time division of all figures is 1 s/div. At this speed, the battery charging current reference is set as 28 A, the maximum charging current; and battery voltage reference is set as 250 V, the rated full-charging voltage. As shown in the figure, when charging control is initiated, the battery current is well controlled with current reference of 28 A. During this CC control period, q-axis current increases in accordance with the rising battery voltage, because the required charging power for constant current is increased by the battery voltage.

Figure 13 shows the results of CC-CV control at various speeds. This experiment was conducted by adjusting the speed of the load motor from 1000 rpm to 3000 rpm; charging current was 15 A, charging voltage was 250 V, and time division was 5 s. Even with sudden change (increase/decrease) in motor speed, CC-CV control is achieved by modifying the regenerative torque with the proposed control method. Note that if battery voltage is increased, the controlled regenerative torque also rises, because the power required for constant battery current control also increases, similar to as shown in Figure 12.

Table 3 shows a comparison between the previous control method by [14] and the proposed one. The charging method using the old charging controller has 89% maximum efficiency; however, with the proposed charging method, maximum efficiency was found to be 92%. The older method used a hysteresis controller for generative and regenerative operations, incurring losses from the DC-link capacitor. However, the proposed control method does not use a DC/DC converter to charge the battery, and, as a result, efficiency is dramatically enhanced.

Table 3. Comparison of maximum efficiency of the two methods.

Max. Efficiency of Previous Control Method [14]	Max. Efficiency of Proposed Control Method
89%	92%

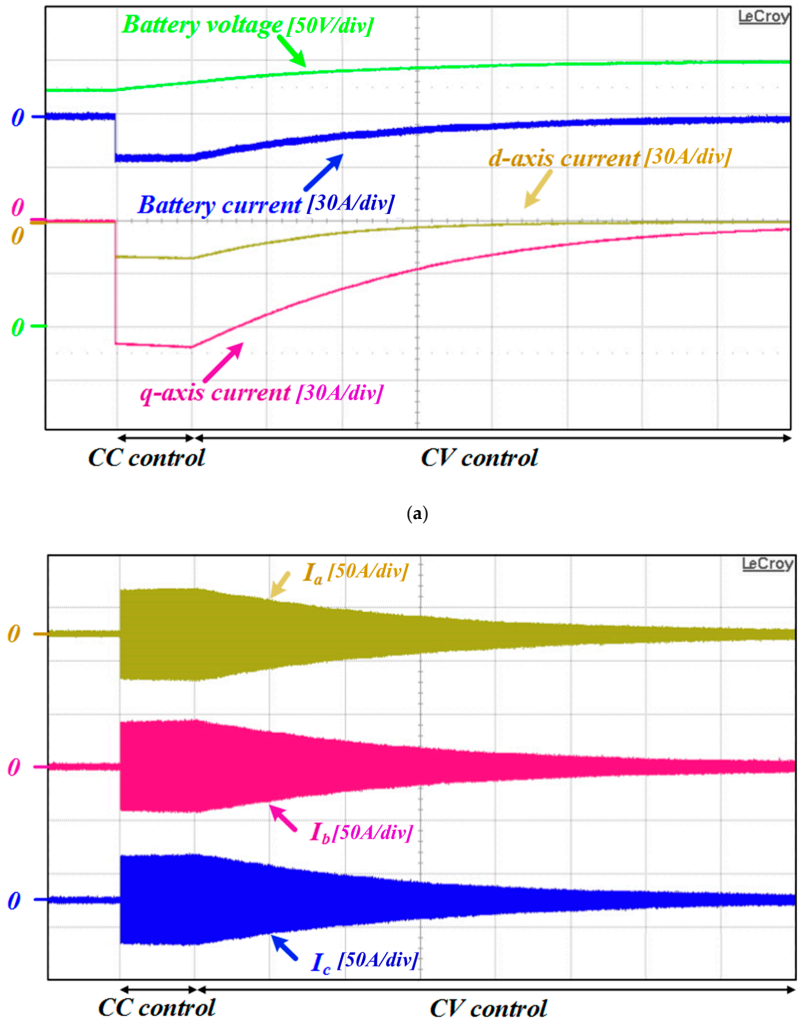

Figure 12. Experimental results of the CC-CV control at 4800 rpm (charging current: 28 A, charging voltage: 250 V). (**a**) dq-axis currents and battery voltage/current; (**b**) phase currents.

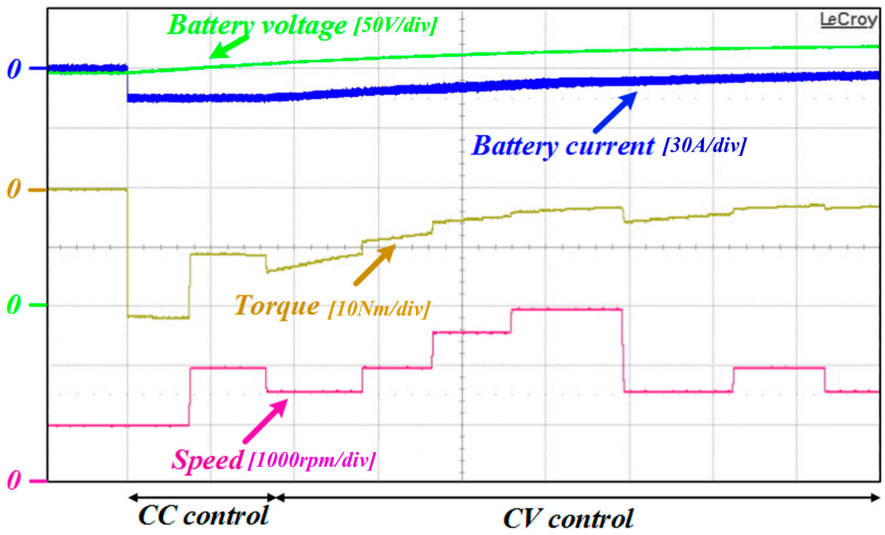

Figure 13. CC-CV control with sudden speed variation (charging current: 15 A, charging voltage: 250 V).

5. Conclusions

This paper proposes regenerative battery current and voltage control methods for PMSM drive. The proposed method controls battery charging using power control. Motor speed and torque can directly affect battery voltage and current; therefore, the proposed control method charges the battery with a CC-CV control, and not a DC-DC converter. A conventional CC-CV control method is achieved by the current sensor of a DC-link or battery; however, inverter switching and the voltage of back-EMF causes ripples in DC-link current, which deteriorate control performance. In contrast, the proposed control method indirectly controls the DC-link current using a power controller, and does not require DC-link current sensing. The proposed method was verified by experiments using maximum power output conditions and varied motor speeds, and was found to be effective for battery charge under varied motor circumstances.

Author Contributions: J.-H.L. and S.-T.K. designed the experiment; J.-H.L. performed the experiment; J.-H.L. analyzed the theory. J.-H.L. wrote the manuscript. J.-H.L. and S.-S.P. participated in research plan development and revised the manuscript. All authors contributed to the manuscript.

Funding: This research was supported by the National Research Foundation of Korea (Grant number: NRF-2018R1C1B6008895); and the Basic Science Research Program through the National Research Foundation of Korea (NRF), funded by the Ministry of Education (NRF- 2016R1A6A1A03013567).

Conflicts of Interest: The authors declare no conflict of interest.

Nomenclature

T_e	Electrical torque
ϕ_{pm}	Permanent magnet flux
L_d, L_q	Inductances of d-/q-axis synchronous frame
L_s	Magnitude of phase inductance
i^r_{ds}, i^r_{qs}	Currents of d-/q-axis synchronous frame
ω_r	Electrical angular velocity
V_{dc}	DC-link voltage
$i_{dc}(t)$	DC-link current
I_{dc}	Effective component of DC-link current
E_{mag}	Back-EMF voltage magnitude
L_s	Phase inductance in the stator
I_a	Magnitude of phase current
$i_a(t), i_b(t), i_c(t)$	a,b,c-phase currents
$v_{an}(t), v_{bn}(t), v_{cn}(t)$	a,b,c-phase back-EMF voltages
P	Number of poles of PMSM
$V_{\max}$	Maximum output voltage of the inverter with SVPWM under linear modulation region

References

1. Wirasingha, S.G.; Emadi, A. Classification and Review of Control Strategies for Plug-In Hybrid Electric Vehicles. *IEEE Trans. Veh. Technol.* **2011**, *60*, 111–122. [CrossRef]
2. Zeraoulia, M.; Benbouzid, M.E.H.; Diallo, D. Electric Motor Drive Selection Issues for HEV Propulsion Systems: A Comparative Study. *IEEE Trans. Veh. Technol.* **2006**, *55*, 1756–1764. [CrossRef]
3. Estima, J.O.; Cardoso, A.J.M. Efficiency Analysis of Drive Train Topologies Applied to Electric/Hybrid Vehicles. *IEEE Trans. Veh. Technol.* **2012**, *61*, 1021–1031. [CrossRef]
4. Ko, J.; Ko, S.; Son, H.; Yoo, B.; Cheon, J.; Kim, H. Development of Brake System and Regenerative Braking Cooperative Control Algorithm for Automatic-Transmission-Based Hybrid Electric Vehicles. *IEEE Trans. Veh. Technol.* **2015**, *64*, 431–440. [CrossRef]
5. Fajri, P.; Lee, S.; Prabhala, V.A.; Ferdowsi, M. Modeling and Integration of Electric Vehicle Regenerative and Friction Braking for Motor/Dynamometer Test Bench Emulation. *IEEE Trans. Veh. Technol.* **2016**, *65*, 1. [CrossRef]

6. Kim, D.; Hwang, S.-H.; Kim, H. Vehicle Stability Enhancement of Four-Wheel-Drive Hybrid Electric Vehicle Using Rear Motor Control. *IEEE Trans. Veh. Technol.* **2008**, *57*, 727–735.
7. Lin, Y.-S.; Hu, K.-W.; Yeh, T.-H.; Liaw, C.-M. An Electric Vehicle IPMSM Drive with Interleaved Front-End DC/DC Converter. *IEEE Trans. Veh. Technol.* **2016**, *65*, 4493–4504. [CrossRef]
8. Cheng, K.W.E.; Divakar, B.P.; Wu, H.; Ding, K.; Ho, H.F. Battery-Management System (BMS) and SOC Development for Electrical Vehicles. *IEEE Trans. Veh. Technol.* **2011**, *60*, 76–88. [CrossRef]
9. Lee, D.-T.; Shiah, S.-J.; Lee, C.-M.; Wang, Y.-C. State-of-Charge Estimation for Electric Scooters by Using Learning Mechanisms. *IEEE Trans. Veh. Technol.* **2007**, *56*, 544–556. [CrossRef]
10. Jiang, J.; Zhang, C.; Wen, J.; Zhang, W.; Sharkh, S.M. An Optimal Charging Method for Li-Ion Batteries Using a Fuzzy-Control Approach Based on Polarization Properties. *IEEE Trans. Veh. Technol.* **2013**, *62*, 3000–3009. [CrossRef]
11. Anseán, D.; González, M.; Viera, J.C.; García, V.M.; Blanco, C.; Valledor, M. Fast charging technique for high power lithium iron phosphate batteries: A cycle life analysis. *J. Power Sources* **2013**, *239*, 9–15. [CrossRef]
12. Vo, T.T.; Chen, X.; Shen, W.; Kapoor, A. New charging strategy for lithium-ion batteries based on the integration of Taguchi method and state of charge estimation. *J. Power Sources* **2015**, *273*, 413–422. [CrossRef]
13. Guo, Z.; Liaw, B.Y.; Qiu, X.; Gao, L.; Zhang, C. Optimal charging method for lithium ion batteries using a universal voltage protocol accommodating aging. *J. Power Sources* **2015**, *274*, 957–964. [CrossRef]
14. Kim, T.-H.; Lee, J.-H.; Won, C.-Y. Design and Control Methods of Bidirectional DC-DC Converter for the Optimal DC-Link Voltage of PMSM Drive. *J. Electr. Eng. Technol.* **2014**, *9*, 1944–1953. [CrossRef]
15. Lee, J.-H.; Jung, D.-Y.; Lee, T.-K.; Kim, Y.-R.; Won, C.-Y. Regenerative Current Control Method of Bidirectional DC/DC Converter for EV/HEV Application. *J. Electr. Eng. Technol.* **2013**, *8*, 97–105. [CrossRef]
16. Yu, F.; Zhu, Z.; Mao, J.; Gu, J. Performance evaluation of a permanent magnet electric-drive-reconfigured onboard charger with active power factor correction. *CES Trans. Electr. Mach. Syst.* **2019**, *3*, 72–80. [CrossRef]
17. Hossain, M.J.; Hossain, M.S.; Hoque, M.A.; Anower, M.S. A Novel Fuzzy Logic Based Flux Weakeneing Speed Control for IPMSM Drive with Variable Direct and quadrature axis inductances. In Proceedings of the 2007 10th International Conference on Computer and Information Technology (ICCIT2007), Dhaka, Bangladesh, 27–29 December 2007.
18. Li, Y.; Zeng, Q.; Wang, C.; Wang, L. Research on Control Strategy for Regenerative Braking of a Plug-In Hybrid Electric City Public Bus. In Proceedings of the 2009 Second International Conference on Intelligent Computation Technology and Automation, Changsha, China, 10–11 October 2009; pp. 842–845.
19. Gao, Y.; Chu, L.; Ehsani, M. Design and Control Principles of Hybrid Braking System for EV, HEV and FCV. In Proceedings of the 2007 IEEE Vehicle Power and Propulsion Conference, Arlington, TX, USA, 9–12 September 2007; pp. 384–391.
20. Lv, M.; Chen, Z.; Yang, Y.; Bi, J. Regenerative braking control strategy for a hybrid electric vehicle with rear axle electric drive. In Proceedings of the 2017 Chinese Automation Congress (CAC), Jinan, China, 20–22 October 2017; pp. 521–525.
21. Jing, H.; Liu, Z.; Liu, J. Wheel slip control for hybrid braking system of electric vehicle. In Proceedings of the Proceedings 2011 International Conference on Transportation, Mechanical, and Electrical Engineering (TMEE), Changchun, China, 16–18 December 2011; pp. 743–746.
22. Basrah, M.S.; Velenis, E.; Cao, D. Four wheel torque blending for slip control in a hybrid electric vehicle with a single electric machine. In Proceedings of the 2015 International Conference on Sustainable Energy Engineering and Application (ICSEEA), Bandung, Indonesia, 5–7 October 2015; pp. 19–24.
23. Jain, A.K.; Mathapati, S.; Ranganathan, V.T.; Narayanan, V. Integrated Starter Generator for 42-V Powernet Using Induction Machine and Direct Torque Control Technique. *IEEE Trans. Power Electron.* **2006**, *21*, 701–710. [CrossRef]
24. Wai, J.; Jahns, T.M. A New Control Technique for Achieving Wide Constant Power Speed Operation with an Interior PM Alternator Machine. In Proceedings of the Conference Record of the 2001 IEEE Industry Applications Conference. 36th IAS Annual Meeting (Cat. No.01CH37248), Chicago, IL, USA, 30 September–4 October 2001; Volume 2, pp. 807–814.